

Topology of nanonetworks grown by aggregation of simplexes with defects

Bosiljka Tadić^{1,6}, Milovan Šuvakov^{2,5}, Miroslav Andjelković³, Geoff J. Rodgers⁴

¹*Department of Theoretical Physics, Jožef Stefan Institute, Jamova 39, Ljubljana, Slovenia*

²*Institute of Physics, University of Belgrade, Pregrevica 118, 11080 Zemun-Belgrade, Serbia*

³*Institute for Nuclear Sciences Vinča, University of Belgrade, 11000 Belgrade, Serbia*

⁴*Brunel University London, Uxbridge Middlesex, UB8 3PH, UK*

⁵*Department of Health Sciences Research, Center for Individualized Medicine, Mayo Clinic, Rochester, Minnesota 55905, USA and*

⁶*Complexity Science Hub Vienna, Josephstadter Strasse 39, Vienna, Austria*

(Dated: December 7, 2021)

Motivated by the relevance of higher-order interactions in quantum physics and materials science at the nanoscale, recently a model has been introduced for new classes of networks that grow by the geometrically constrained aggregation of simplexes (triangles, tetrahedra and higher-order cliques). Their key features are hyperbolic geometry and hierarchical architecture with simplicial complexes, which can be described by the algebraic topology of graphs. Based on the model of chemically tunable self-assembly of simplexes [Šuvakov et al., Sci.Rep 8, 1987 (2018)], here we study the impact of defect simplexes on the course of the process and their organisation in the grown nanonetworks for varied chemical affinity parameter and the size of building simplexes. Furthermore, we demonstrate how the presence of patterned defect bonds can be utilised to alter the structure of the assembly after the growth process is completed. In this regard, we consider the structure left by the removal of defect bonds and quantify the changes in the structure of simplicial complexes as well as in the underlying topological graph, representing 1-skeleton of the simplicial complex. By introducing new types of nanonetworks, these results open a promising application of the network science for the design of complex materials. They also provide a deeper understanding of the mechanisms underlying the higher-order connectivity in many complex systems.

I. INTRODUCTION

In recent years, the application of graph theory to analyse complex patterns in empirical data has revolutionised research in various interdisciplinary sciences. Some well-known examples include emotion-driven online dynamics with co-evolving networks of users and posts [1] and mapping brain imaging data (see recent related [2] and references there). However, the use of graphs for mapping certain problems in physics and materials science is still in its infancy [3–8]. In this case, more profound knowledge of the physics and chemistry of the problem helps to appropriately identify the nodes and edges of the structure, that often refers to the phase space of the system rather than a real-space structure.

In materials science, complex structures made of nanoscale objects often correlate with an increased functionality [9, 10]. Processes of self-assembly are widely used to grow such systems, where the addition of each object to the growing structure obeys certain rules and locally minimises the energy [11–13]. Therefore, the use of mathematical concepts [14] and graph representations [3] are highly desirable for both the design and characterisation of the nanostructured assemblies. In this context, real-space networks are visualised, for example, with the nanoparticles as nodes and edges representing a kind of chemical binding [15] or another association between them that is relevant for the problem in question. For example, the network representations of the conducting nanoparticle films have been studied in [16–18]. The use of graph theory has enabled the description and differentiation of the structures that promote enhanced conduction via single-

electron tunnellings between nanoparticles spaced within the quantum tunnelling radius in the direction of the current.

Cooperative self-assembly [19–21], where the preformatted group of particles attach to a growing structure represents a higher level of the self-assembly processes, and opens an avenue towards new types of *materials inspired by mathematics* [14, 22]. Colloids with “valence” and directional bonding are a physical reality [23], particles with $n \in [1, 7]$ active patches were created by 2-stage swelling of the minimal moment clusters, and subsequent DNA functionalization, resulting in different forms as spheres, dumbbells, triangles, tetrahedra and higher-order structures. In these processes, the geometrical-compatibility constraints of the binding forms with the growing structure play an important role, apart from the chemical affinity between the structure and the binding nanoparticles. Recently, we developed a model with the appropriate self-assembly rules [22, 24], where the building blocks are suitably described by simplexes, i.e., edges, triangles, tetrahedrons, and cliques of higher orders. A prominent feature of these structures is a hierarchical architecture of simplicial complexes, which is accessible to the methods of the algebraic topology of graphs [25, 26], as well as emergent hyperbolicity in the graph’s metric space [27–30].

In this work, based on the model in [22], we extend the study of the cooperative self-assembly by considering the presence of defect simplexes and describe the impact of defect bonds on the assembled nanonetworks. Specifically, we show how the presence of simplexes with a defect edge can alter the course of the process leading to the structure with not-random patterns of defect bonds and changed topological

features of the assembly, depending on the size of the binding simplexes and the chemical affinity parameters. We further demonstrate how the patterned defect bonds can be utilised to alter the structure in the already grown assembly. Changes in the topological properties of the assemblies are quantified using the algebraic topology analysis of simplicial complexes, as well as by determining the hyperbolicity parameter of the underlying graph.

II. THE MODEL AND GROWTH OF NANONETWORKS WITH DEFECTS

Following the original model [22], we consider the assembly of simplexes that are full graphs (cliques) of n vertices. Starting from an initial simplex the new simplex of the size driven from the probability $p_n \sim n^{-\alpha}$ (we fix $\alpha = 2$ if not specified) is attached to the growing structure by sharing one of its faces. Notice that a simplex of n vertices possesses faces as sub-simplexes of all orders $q = 0, 1, 2, 3 \dots q_{max} - 1$ from the vertex to the largest sub-simplex, where $q_{max} = n - 1$ indicates the order of the simplex. Determining the face to be shared depends first on the number of geometrically compatible sites in the current structure (geometrical compatibility constraint). Moreover, when a face of the order q is shared with an already existing simplex in the growing structure, the remaining $n_a = q_{max} - q$ vertices will be added to the system as a formatted group of nanoparticles. The affinity of the system towards the addition of a group is described by the chemical affinity parameter v [22, 31], which modifies the probability defined based on the geometry factor alone, see Eq. (1). Specifically, for a large negative v , the system likes the addition of particles, which results in sharing a minimal face, that is a single node. In this limit, the cliques are effectively repelling each other. Whereas, in the opposite limit, with a large $v > 0$, a single node is preferably added; thus, the added clique shares its largest face with a previous compatible structure [22].

Here, we allow that a simplex to be added to the structure can, with a finite probability p , have a bond that differs from the other bonds, i.e., a defect; the presence of such defect bonds affects the geometrical compatibility factors, as explained below. More precisely, we have

$$P(q_{max}, q; p, t) = \frac{c_q(p, t) e^{-v(q_{max}-q)}}{\sum_{q=0}^{q_{max}-1} c_q(p, t) e^{-v(q_{max}-q)}} \quad (1)$$

which defines the normalised probability that a clique of the order q_{max} will attach along its face of the order q , subject of the presence of a defect edge. Specifically, a defect edge of the arriving clique can nest along another defect edge on the network, else the adjacent nodes are shared, while the straight (pure) edges align along the straight edges in the geometrically compatible shapes. Therefore, at the evolution time t , the number of the geometrically similar docking sites $c_q(p, t)$ of the searched order q also depends on the potential defect edge to match the defect in the face of the newly added clique. In this way, the presence of defects that are already built in the

structure affects future binding events. Fig. 1 illustrates the impact of the presence of defect edges in the process of self-assembly. Note that the number of geometrically compatible sites for docking along with the faces with pure bonds changes even if a small number of defect bonds are present. For example, to add a new pure triangle along its largest face, i.e., an edge, to the structure in the middle, apart from the tree bonds in the top triangle, we can have only two more candidates, the bonds 3-4 and 3-8. In contrast, 15 bonds are available in the case when the same structure consists of only pure bonds. Some examples of grown assemblies with varied parameters are shown in Fig. 2 and in Fig. 3.

The impact of defect edges for a given p also depends on the size and the dispersion of the attaching cliques, and the binding affinity v . When the affinity among cliques is significant, such that they intend to share their maximal faces, the aggregation of defect edges is more effective (see Fig. 3), leading to stronger aggregation of defect bonds and constraints to the remaining structure. Notably, defect bonds make a particular pattern. These effects are especially pronounced in the case of small cliques, where a defect edge provides a more severe restriction on the binding of the remaining faces. In the case of purely geometrical aggregation, $v = 0$, the defect edges at sufficiently large concentration form tree-like structures and "highways" through the graph. Consequently, the grown network with defect simplexes is different from the case when the simplexes with equal edges were used (i.e., $p = 0$), see Table I. In the following, we employ Q-analysis [26, 32, 33] to quantitatively describe the organisation of simplicial complexes in various aggregates grown in the presence of defect bonds, in comparison with the case $p = 0$. We also analyse the changes in the structures caused by the removal of the defect bonds.

III. Q-ANALYSIS & IMPACT OF DEFECT BONDS ON THE ARCHITECTURE OF NANONETWORKS

In this context, a simplex of the order $q_{max} = n - 1$ is a full graph of n vertices. In a simplicial complex, two simplexes are q -connected if they share a face of the order q , i.e., they have at least $q + 1$ shared nodes. The dimension of the considered simplicial complex equals the dimension of the largest clique $q_{max} + 1$ belonging to that complex. To describe the structure of simplicial complexes at different topology levels $q = 0, 1, 2 \dots q_{max}$, Q-analysis uses notation from the algebraic topology of graphs [26, 34, 35]. Specifically:

- the first structure vector (FSV) components $\{Q_q\}$ denote the number of q -connected components;
- the second structure vector (SSV) components $\{n_q\}$ corresponds to the number of simplexes of the order greater than or equal to q ;
- then the third structure vector (TSV) component q is determined as $\hat{Q}_q \equiv 1 - Q_q/n_q$ measuring the degree of connectivity at the topology level q among the simplexes of the order higher than q .

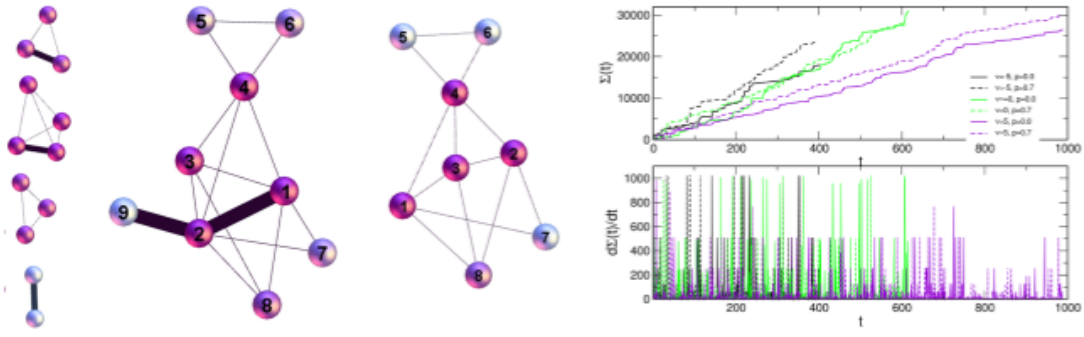


FIG. 1: Left: Illustration of the aggregation of simplexes with defect edges, indicated by thick lines. For example, assuming that the structure shown in the middle emerged from the type of simplexes shown on the left, we observe the following sequence of events: Starting from a defect tetrahedron with the vertices 1-2-3-4, a pure triangle 4-5-6 is attached sharing the node 4, then a defect triangle 1-2-7 is attached sharing the defect edge 1-2, following by the attachment of another defect tetrahedron 1-2-3-8 by sharing its defect triangle face with the previous structure; eventually, a defect dumbbell 9-2 is attached sharing its defect face, the node 2. The connected structure that remains after removal of two defect edges is shown on the right of the figure. Right: For the distribution of the attaching simplexes in the range $n \in [2, 10]$, the evolution of the number of simplexes and faces in the graph $\Sigma(t)$ until the number of nodes reaches 1000. Three values of the affinity parameter v are considered, shown in the legend, combined with the probability $p = 0.7$ of a defect bond in simplexes and simplexes with all pure bonds $p = 0.0$. The lower panel shows the change in the number of simplexes in time.

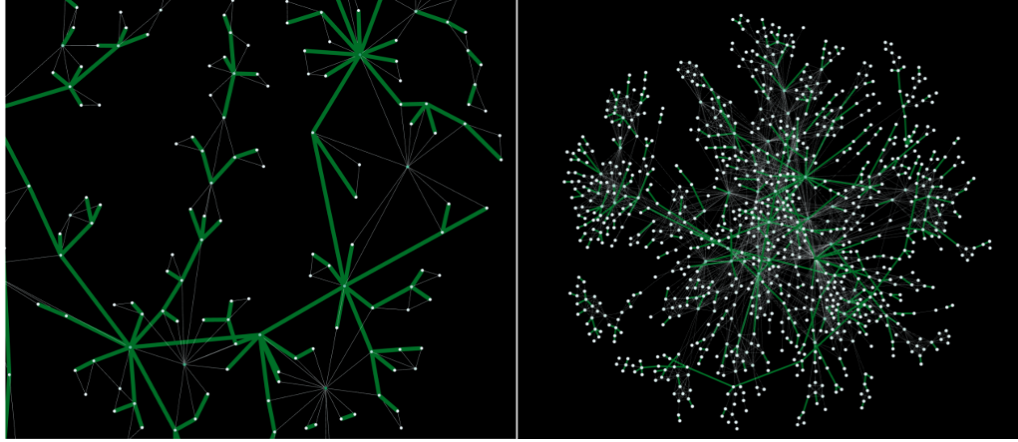


FIG. 2: Close-up of the structure of assembly of triangles (left) and the assembly of the distributed clique sizes $n \in [2, 10]$ according to $\sim n^{-2}$ (right) for strictly geometric aggregation ($v = 0$) and 70% defect simplexes. Defect edges are shown as thick (green) lines.

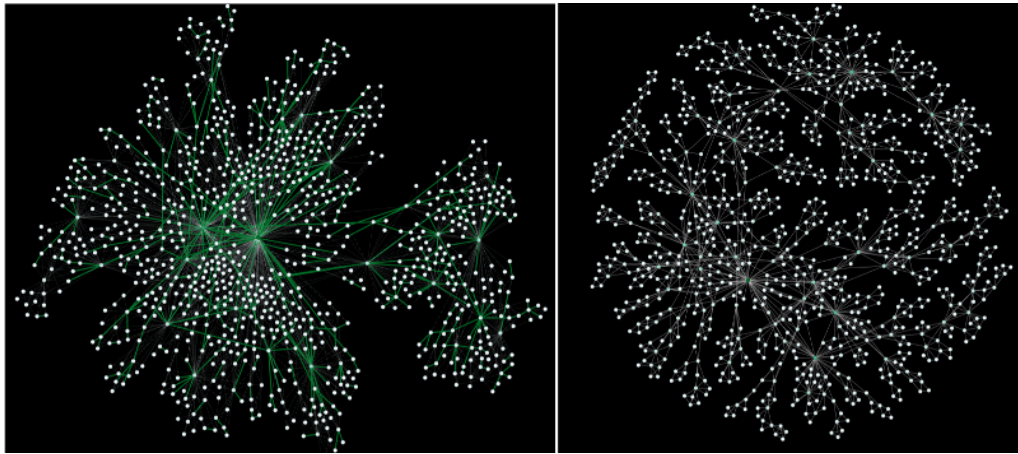


FIG. 3: An example of the nanonetwork with defect bonds (thick green edges) assembled at affinity $v = +5$ from tetrahedra with the probability of a defect bond $p = 0.5$ (left), and the structure obtained after removing the defect bonds (right).

Using the Bron-Kerbosch algorithm [36] we construct the incidence matrix $\Lambda(G)$ of the graph G , starting from its adja-

cency matrix. The incidence matrix contains complete information about all present simplexes as well as the vertices that belong to each simplex. Thus the components of these structure vectors can be determined from the corresponding incidence matrix $\Lambda(G)$. Further characterisation of the architecture of simplicial complexes is provided by the quantity f_q , which is defined [37] as the number of simplexes and faces at the topology level q .

Furthermore, we compute these topology features for the assembly that remains after the removal of defect bonds. Notice that the removal of the defect bonds changes the structure of the assembly by breaking the simplexes in which such bonds were built-in. For example, cf. Fig.1, a defect tetrahedron breaks into two triangles that are attached along the common edge when the defect bond is removed. The effects of the defect bond removal correlate with the size of the original cliques. More precisely, the following rule applies:

- a clique of the order q_{max} with a defect bond breaks into two cliques of the order $q_{max} - 1$;
- these new cliques are attached along their largest face, that is they share a face of the order $q_{max} - 2$.

Fig. 4 and Fig.5 show these structural properties of a few representative aggregates of simplexes obtained with/without defect bonds. Notably, the aggregation of defect faces causes those made of pure bonds to spread, which results in higher values of f_q for a finite concentration of defect bonds p , as compared with $p = 0$. This principle applies, although the values are different, for all aggregates at different values of parameter ν . One should also notice that the highest point of f_q correlates with the number of simplexes that need to be added to complete a given number of vertices, here $N \geq 1000$, which is considerably different for different ν , cf. Fig. 1, right. With the removal of the defect bonds, generally, we have a smaller number of simplexes and faces, resulting in the proportional decrease of f_q at all q levels, in comparison with the original structure with defects. The effects are more pronounced in the dense structure of cliques, corresponding to $\nu > 0$, cf. Fig. 4, than in the structures with sparsely connected cliques (for $\nu < 0$ and partly $\nu = 0$).

In the structure vectors, shown in Fig. 5, notice that the aggregates grown with or without defect represent one connected component, then the FSV component $Q_0 = 1$. The peak in the FSV at $q = 1$ and the decay at larger $q < 10$ reflects the actual distribution of the size $n \in [2, 10]$ of the attaching cliques; the distribution $f_n \sim n^{-2}$ favours dumbbells as compared with higher-order cliques up to the 10-cliques. The total number of cliques, which is given by the 0th components of the SSV, given in the middle row in Fig. 5, is significantly more prominent in compact structures ($\nu = +5$) than in the sparse assembly of cliques grown at $\nu = 0$ and $\nu = -5$. This observation is compatible with the growth process depicted in Fig. 1. In the presence of defect cliques, the number of q -connected components, as well as the total number of cliques from the level q upwards, differ from the case of a structure with pure simplexes, in particular in the range of large and intermediate q -values. The components of TSV indicate that in

the compact regions of the graph (i.e., in the case $\nu = +5$ and partly in $\nu = 0$), the large cliques with defect bonds are more weakly connected than in the pure-simplexes structure. However, in the range $q \in [2, 6]$ for $\nu = +5$ and $q \in [1, 4]$ for the case $\nu = 0$, the connectivity exceeds the curve of TSV for the structure without defects. Meanwhile, in the case $\nu = -5$, the cliques of all sizes share a single node, therefore they appear to be disconnected already at the level $q = 1$, cf. TSV in the lower right panel in Fig. 5.

With the removal of defect bonds, the number of large cliques gradually decreases, while the number of intermediate and small cliques results as a balance between breaking the initially present defect cliques of that order and the appearance of new ones from the broken defect cliques of one order higher. Consequently, the FVS changes such that Q_0 increases because of broken bonds, some separate graph parts can occur. The changes are most dramatic in the case of $\nu < 0$. Following a broken bond in a clique of order nine, we have two cliques of the order eight that are sharing a clique of the order seven, and so on, as explained above. Consequently, non-trivial connectivity appears among these newly generated cliques at all levels $q \in [1, 8]$, as shown in the lower right panel of Fig. 5, even though the originally built-in cliques repelled each other such to share a single vertex. A similar effect occurs in the sparse areas of the structure grown in the absence of chemical factors ($\nu = 0$). The effects are proportional to the probability of a defect bond p , which decides the actual number of defect bonds in the grown structure, depending on ν (see Table I). In the following, we analyse how the changed architecture of simplicial complexes due to breaking defect bonds affects the hyperbolicity and other features of the topological graph.

IV. CHANGES OF HYPERBOLICITY INDUCED BY THE REMOVAL OF DEFECT BONDS

As mentioned in the Introduction, the assembly of cliques possesses a *negative curvature in the graph's metric space*, which is endowed with the shortest-path distance. Hence, the generalised Gromov's 4-point hyperbolicity criterion can be applied to characterise it. Specifically, the graph G is hyperbolic *iff* there is a constant $\delta(G)$ such that for any four vertices $\{A, B, C, D\}$ of the graph, the relationships between the sums of distances between distinct pairs of these nodes $d(A, B) + d(C, D) \leq d(A, C) + d(B, D) \leq d(A, D) + d(B, C)$ implies that

$$\delta(A, B, C, D) = \frac{\mathcal{L} - \mathcal{M}}{2} \leq \delta. \quad (2)$$

Here $d(U, V)$ indicates the shortest-path distance and we denoted the largest $\mathcal{L} = d(A, D) + d(B, C)$ and the middle value $\mathcal{M} = d(A, C) + d(B, D)$. Observing that the upper bound of the expression in (2) is $(\mathcal{L} - \mathcal{M})/2 \leq d_{min}$, where $d_{min} = \min\{d(A, B), d(C, D)\}$ enables us to determine the hyperbolicity parameter $\delta(G)$ by plotting $(\mathcal{L} - \mathcal{M})/2$ against d_{min} and investigating the worst case growth of the dependence. For each graph, using its adjacency matrix, we first compute the

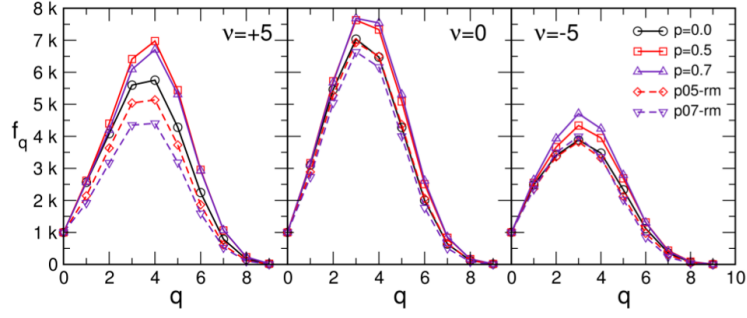


FIG. 4: f_q vs q for the pure ($p = 0$) and defect network ($p=0.7, 0.5$) and the network obtained by removal of defect bonds ($p=0.7$ -rmw2, p05-rmw2) for three values of $v = 5, 0, -5$, left to right.

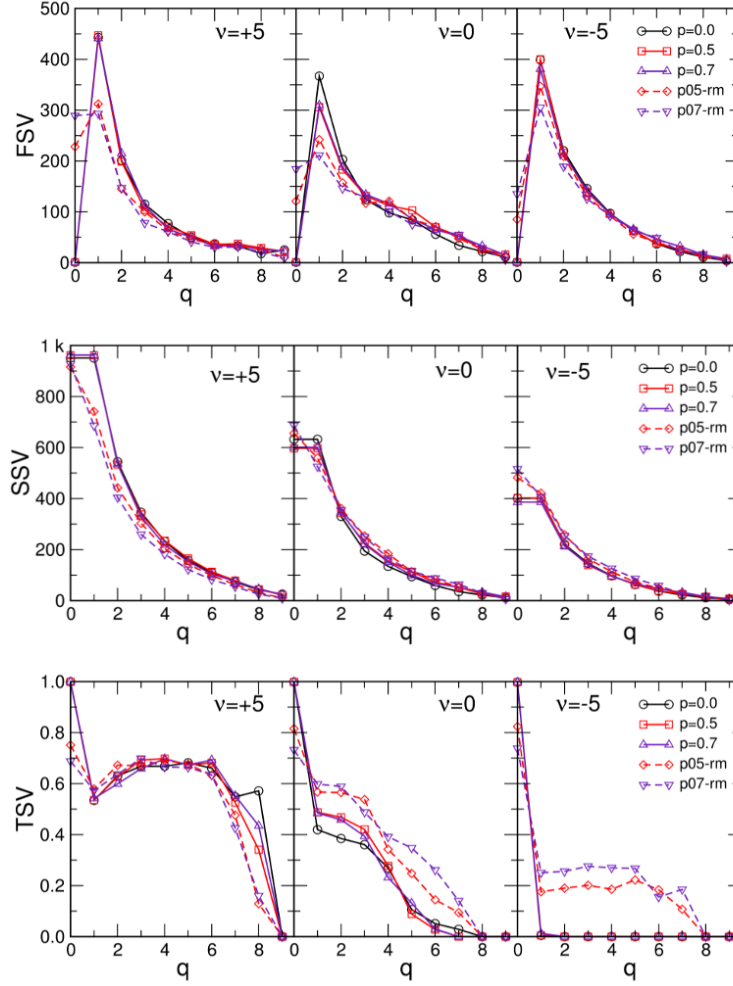


FIG. 5: Components of the first (FSV), second (SSV) and third (TSV) structure vector (top-to-bottom row) against the topology level q for the pure ($p=0.0$) and defect network ($p=0.5$ and 0.7) and the network obtained by removal of defect bonds (p05-rmw2, p07-rmw2) for three values of $v = 5, 0, -5$, indicated on each panel.

matrix of distances between all pairs of nodes. Then, by sampling a large number of sets of nodes for the 4-point condition (2) we determine and plot the largest δ against the corresponding distance d_{min} ; the maximum observed value of all δ_{max} determines the graph's hyperbolicity parameter $\delta(G)$.

For the graphs with a small hyperbolicity parameter, it is known [28, 30, 38] that the upper bound of the hyperbolicity parameter is related to a specific subadjacent structure; for example [39], the presence of an isometric cycle C_n of the length $n \geq 3$ would lead to $\delta(C_n) = \lfloor n/4 \rfloor - \frac{1}{2}$, if $n \equiv 1 \pmod{4}$, else

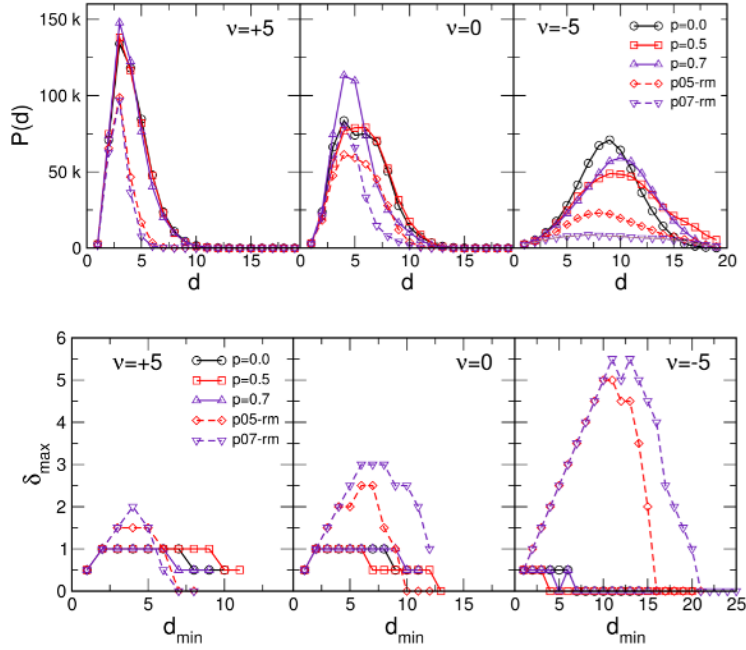


FIG. 6: The distance distribution $P(d)$ vs d , and δ_{max} vs d_{min} for the pure ($p = 0$) and defect network ($p=0.7,0.5$) and the network obtained by removal of defect bonds (p05-rmw2,p07-rmw2) for three values of $v = 5,0,-5$, left to right.

$\delta(C_n) = \lfloor n/4 \rfloor$. Similarly, since the cliques are ideally hyperbolic ($\delta_{clique} = 0$), a combination of cliques that are apart at a small distance i causes the increase of the hyperbolicity parameter by an integer [30], i.e., $\delta_{clique} + i$.

The network growth in our algorithm by attaching a new clique such that it shares a face with another previously present clique in the system, immediately implies that their hyperbolicity parameter cannot exceed unity. That is, these are 1-hyperbolic graphs [22], as also confirmed by a direct computation, see Fig. 6. The same conclusion also applies to the structure grown with the defect cliques, as long as the cliques are complete. However, by removing the defect bonds, the cliques that contained them break into smaller cliques that appear to be differently attached to the rest of the graph. Moreover, holes of different sizes and dimensions can occur. Consequently, we have an increase of the hyperbolicity parameter of the whole graph, due to the presence of longer cycles and increased distances between the newly observed cliques.

Fig. 6 shows the distribution of distances in the case of pure simplexes and in the presence of defect cliques, and how it changes by the removal of defect bonds for varied parameters p and v . Notice that the distribution of distances between pairs of nodes changes due to the presence of defect bonds. In contrast to the dense graphs (for $v = +5$), where the most probable distance remains three, in the sparse graphs (at $v = 0$ and especially at $v = -5$) the most probable distances are larger than in the case without defects. Similarly, these graphs experience the most dramatic changes in the distance distributions when the defect bonds are removed. The diameter of the graph (referring to the largest connected component) also

changes, cf. table I.

The lower panels show the hyperbolicity parameter δ_{max} for the corresponding graphs. As expected, $\delta_{max} = 1$ for all graphs grown by the attachment of cliques rule with and without defect bonds, for all v values. However, when the defect bonds are removed, the changed organisation of simplexes, as described above, leads to the appearance of holes and long cycles, which results in the increased values of δ_{max} . The increase strongly depends on v at which the graph with defect simplexes is grown. More precisely, in compact structures, the hyperbolicity parameter reaches the values $3/2$ or 2 , compatible with the subjacent structures with increased distances between the cliques. On the other hand, a substantial increase of δ_{max} in the sparse structures, reaching the values 3 for $v = 0$ and 5.5 for $v = -5$ and the considered concentration of the removed bonds, can be related to the appearance of long cycles.

V. SUMMARY AND DISCUSSION

We have introduced a model for self-assembly of simplexes in the presence of a defect bond. The model allows for the variation of the probability of a defect bond in the attaching simplexes in conjunction with their size n and the chemical affinity v , leading to a rich variety of resulting assemblies. In this study, we consider a fixed probability p and the sizes distributed according to $p_n \sim n^{-2}$ in the range $n \in [2, 10]$. We have shown how the presence of defect bonds can tune the structure of simplicial complexes as well as the underlying topological graph. The results of the quantitative analysis in Fig. 4, Fig. 5 and Fig. 6, show that the model provides the

TABLE I: Graph measures of the assemblies of simplexes of the size $n \in [2, 10]$ distributed as $\propto n^{-2}$ and the probability of defect bond p , for three representative values of the affinity parameter $v = \pm 5$, and 0. The properties of graphs with removed pattern of defect edges, (0.7-db) and the graph when the same number of edges c is removed at random (rand-c) are also shown. The effective concentration of defect edges c , the average degree $\langle k \rangle$, path length $\langle \ell \rangle$ and clustering coefficient $\langle Cc \rangle$, graph's modularity mod , diameter D , spectral dimension d_s , all computed for the graph size $N = 5000$ nodes. Additional properties computed for the graphs of the same parameters but $N = 1000$ nodes are the hyperbolicity parameter δ_{max} , and the topology level q^* at which the connectivity (third structure vector TSV) between the simplexes drops to zero, and the connectivity at the level before $q^* - 1$.

v	p	c	$\langle k \rangle$	$\langle \ell \rangle$	$\langle Cc \rangle$	mod	D	δ_{max}	q^*	$TSV(q^* - 1)$
+5	0.0	0	5.005	4.475	0.601	0.524	18	1	9	0.057
	0.7	0.271	5.115	4.197	0.602	0.556	19	1	9	0.435
	0.7-db	0	5.0671	3.025	0.774	0.414	11	2.0	9	0.160
	rand-c	0	4.162	3.971	0.492	0.517	14	3.0	6	0.079
0	0.0	0	5.988	6.209	0.714	0.882	17	1	8	0.0285
	0.7	0.149	5.933	6.256	0.721	0.872	17	1	7	0.0298
	0.7-db	0	6.124	5.719	0.742	0.867	17	3.0	8	0.141
	rand-c	0	5.231	7.027	0.610	0.883	23	3.0	7	0.024
-5	0.0	0	5.075	13.213	0.813	0.972	32	1	2	0.005
	0.7	0.109	5.270	11.788	0.825	0.966	27	1	2	0.0129
	0.7-db	0	5.223	10.417	0.783	0.975	31	5.5	8	0.185
	rand-c	0	4.625	14.751	0.730	0.973	31	4.5	7	0.218

framework to grow a rich structure of simplicial complexes with the possibility to control both the process of the growth of the assembly as well as to change it by influencing the defect edges after the growth is completed. In this study, we have demonstrated how the removal of defect bonds leads to the altered structure of simplicial complexes; moreover, the presence of holes and cycles in these transformed assemblies are associated with the increase of the graphs hyperbolicity parameter. Some standard graph properties and their hyperbolicity as well as measures indicating the connectivity between simplexes are listed in the table I for the representative sets of parameters.

Remarkably, the defect bonds make non-random patterns—tree-like structures in the graphs, even though no long-range forces are present. The apparent attraction among defects is primarily related to the geometrical constraints for the docking of simplexes; thus, it depends on the size of simplexes and the chemical affinity towards new vertices. Therefore, the removal of patterns of defect bonds has a profound effect on the structure of simplicial complexes, as discussed above. These patterns also shape the graph's properties differently, as compared with the case when the same number of defect bonds are randomly distributed, cf. table I.

In summary, we have introduced new classes of networks that evolve by self-assembly of simplexes with different shapes and types of bonds. The variations of the parameters governing the process of self-assembly allow different types of structures to grow from sparsely separated simplexes to compact structure with large simplicial complexes, and the

possibility to modify their organisation by affecting a specific type of bonds. These approaches are suitable for designing new classes of nano-structured assemblies and for their quantitative characterisation beyond the standard pairwise interactions. The presented study also offers a deeper understanding of the mechanisms beyond the higher-order connectivity that lead to the occurrence of simplicial complexes in many other complex systems, from human connectomes [2] to patterns representing the brain-to-brain coordination [40] and online social dynamics [41, 42], as well as a variety of problems in physics [5–7, 37, 43].

Acknowledgments

Authors acknowledge the financial support from the Slovenian Research Agency under the program P1-0044 and from the Ministry of Education, Science and Technological Development of the Republic of Serbia, under the projects OI 171037, III 41011 and OI 174014.

Author contributions statement

B.T. and M.S. designed research, M.S. contributed program tools, M.A., B.T., M.S., G.J.R. performed simulations and analysed data, B.T. produced figures and wrote the manuscript, all authors reviewed the manuscript.

[1] Tadić B, Gligorijević V, Mitrović M, Šuvakov M. 2013 Co-evolutionary mechanisms of emotional bursts in online social dynamics and networks. *Entropy* **15** 5084–5120.
 [2] Tadić B, Andjelković M, Melnik R. 2019 Functional geometry

of human connectomes. *Scientific Reports* **9** 12060.
 [3] Živković J, Tadić B. 2013 Nanonetworks: The graph theory framework for modeling nanoscale systems. *Mathematics of Quantum and Nanotechnologies NanoMMTA* **2** 30–48.

- [4] Ikeda S, Kotani M. 2015 *A new direction in mathematics for materials science*. Springer, Tokyo.
- [5] Bianconi G, Rahmede C, Wu Z. 2015 Complex quantum network geometries: Evolution and phase transitions. *Phys. Rev. E* **92** 022815.
- [6] Cinardi N, Rapisarda A, Bianconi G. 2019 Quantum statistics in network geometry with fractional flavor. *arXiv:1902.10035v1*, pages 1–60.
- [7] Tadić B, Andjelković M, Šuvakov M. 2016 The influence of architecture of nanoparticle networks on collective charge transport revealed by the fractal time series and topology of phase space manifolds. *Journal of Coupled Systems and Multiscale Dynamics* **4** 30–42.
- [8] Krivovichev SV. 2004 Combinatorial topology of salts of inorganic oxoacids: zero-, one- and two-dimensional units with corner-sharing between coordination polyhedra. *Crystallography Reviews* **10** 185–232.
- [9] Pelaz B, *et al.* 2012 The state of nanoparticle-based nanoscience and biotechnology: Progress, promises, and challenges. *ACS Nano* **6** 8468–8483.
- [10] Fan X, *et al.* 2016 Review of adaptive programmable materials and their bioapplications. *ACS Appl. Mater. Interfaces* **8** 33351–33370.
- [11] Whitesides GM, Grzybowski B. 2002 Self-assembly at all scales. *Science* **295** 2418–24212.
- [12] Xiaodong Xing X, *et al.* 2016 Probing the low-energy structures of aluminum-magnesium alloy clusters: a detailed study. *Phys. Chem. Chem. Phys.* **18** 26177–26183.
- [13] Boles MA, Michael Engel M, Talapin DV. 2016 Self-assembly of colloidal nanocrystals: From intricate structures to functional materials. *Chemical Reviews* **116** 11220–11289.
- [14] Ikeda S, Kotani M. 2016 Materials inspired by mathematics. *Science and Technology of Advanced Materials* **17** 253–259.
- [15] Šuvakov M, Bosiljka Tadić B. 2009 Collective charge fluctuations in single-electron processes on nanonetworks. *Journal of Statistical Mechanics: Theory and Experiment* **2009(02)** P02015.
- [16] Blunt MO, *et al.* 2007 Charge transport in cellular nanoparticle networks: Meandering through nanoscale mazes. *Nano Letters* **7** 855–860.
- [17] Blunt MO, *et al.* 2010 *Patterns and pathways in nanoparticle self-assembly*. Oxford University Press, Oxford, New Yorks.
- [18] Šuvakov M, Bosiljka Tadić B. 2010 Modeling collective charge transport in nanoparticle assemblies. *Journal of Physics: Condensed Matter* **22** 163201.
- [19] Gu Y, *et al.* 2013 Collective alignment of nanorods in thin newtonian films. *Soft Matter* **9** 8532–8539.
- [20] Ahn S, Lee SJ. 2014 Hierarchical nanoparticle clusters induced by block copolymer self-assembly. *Soft Matter* **10** 3897–3905.
- [21] Liu S, Yu J. 2008 Cooperative self-construction and enhanced optical absorption of nanoplates-assembled hierarchical bi2wo6 flowers. *Journal of Solid State Chemistry* **181** 1048–1055.
- [22] Šuvakov M, Andjelković M, Tadić B. 2018 Hidden geometries in networks arising from cooperative self-assembly. *Scientific Reports* **8** 1987–1–10.
- [23] Wang Y, *et al.* 2012 Colloids with valence and specific directional bonding. *Nature* **491** 51.
- [24] Šuvakov M, Andjelković M, Bosiljka Tadić B. 2017 Applet: Simplex aggregated growing graph (<http://suki.ipb.rs/ggraph/>).
- [25] Jonsson J. 2008 *Simplicial Complexes of Graphs*. Lecture Notes in Mathematics, Springer-Verlag, Berlin.
- [26] Beaumont JR, Gattrell AC. 1982 *An Introduction to Q-Analysis*. Geo Abstracts, Norwich-Printed by Edmund Nome Press, Norwich.
- [27] Rodriguez JM, Touris E. 2004 Gromov hyperbolicity through decomposition of metric spaces. *Acta Math. Hungar.* **103** 53–84.
- [28] Bermudo S, Rodríguez JM, Rosario O, Sigarreta JM. 2016 Small values of the hyperbolicity constant in graphs. *Discrete Mathematics* **339** 3073 – 3084.
- [29] Bermudo S, Rodríguez JM, Sigarreta JM, Vilaire JM. 2013 Gromov hyperbolic graphs. *Discrete Mathematics* **313** 1575 – 1585.
- [30] Cohen N, Coudert D, Ducoffe G, Lancin A. 2017 Applying clique-decomposition for computing gromov hyperbolicity. *Theoretical Computer Science* **690**(Supplement C) 114 – 139.
- [31] Šuvakov M, Tadić B. 2006 *Topology of Cell-Aggregated Planar Graphs*, pages 1098–1105. Springer Berlin Heidelberg, Berlin, Heidelberg.
- [32] Bandelt HJ, Chepoi V. 2008 Metric graph theory and geometry: a survey, in Goodman JE, Pach J, Pollack R, eds. "Surveys on discrete and computational geometry: Twenty years later". volume **453**, Providence, RI: AMS .
- [33] Maletić S, Yi Zhao Y. 2017 *Simplicial Complexes in Complex Systems: The Search for Alternatives*. Harbin Institute of Technology, Harbin, Peoples Republic of China, first edition.
- [34] Atkin RH. 1976 An algebra for patterns on a complex, ii. *International Journal of Man-Machine Studies* **8** 483 – 498.
- [35] Johnson J. 1981 Some structures and notation of q-analysis. *Environment and Planning B: Planning and Design* **8** 73–86.
- [36] Bron C, Kerbosch J. 1973 Finding all cliques of an undirected graph. *Comm ACM* **16** 575–577.
- [37] Andjelković M, Gupte N, Bosiljka Tadić B. 2015 Hidden geometry of traffic jamming. *Phys. Rev. E* **91** 052817.
- [38] Carballosa W, Pestana D, Rodríguez JM, Sigarreta JM. 2014 Distortion of the hyperbolicity constant in minor graphs. *Electronic Notes in Discrete Mathematics* **46** 57 – 64.
- [39] Wu Y, Zhang C. 201 Hyperbolicity and chordality of a graph. *The Electronic Journal of Combinatorics* **18** P43.
- [40] Tadić B, Andjelković M, Boshkoska BM, Levnajić Z. 2016 Algebraic topology of multi-brain connectivity networks reveals dissimilarity in functional patterns during spoken communications. *PLOS ONE* **11** e0166787.
- [41] Andjelković M, Tadić B, Maletić S, Rajković M. 2015 Hierarchical sequencing of online social graphs. *Physica A: Statistical Mechanics and its Applications* **436** 582–595.
- [42] Andjelković M, *et al.* 2016 Topology of innovation spaces in the knowledge networks emerging through questions-and-answers. *PLOS ONE* **11** e0154655.
- [43] Senyuk B, *et al.* 2015 Geometry-guided colloidal interactions and self-tiling of elastic dipoles formed by truncated pyramid particles in liquid crystals. *Phys. Rev. E* **91** 040501.